Proceedings Paper:
House, D, Skene, C orcid.org/0000-0003-0994-2013, Ribeiro, JHM et al. (2 more authors) (2022) Sketch-Based Resolvent Analysis. In: AIAA AVIATION 2022 Forum. AIAA AVIATION 2022 Forum, 27 Jun - 01 Jul 2022, Chicago, IL, USA. American Institute of Aeronautics and Astronautics . ISBN 978-1-62410-635-4

https://doi.org/10.2514/6.2022-3335

Sketch-Based Resolvent Analysis

Dylan House*
University of California, Los Angeles, CA 90095, USA

Calum S. Skene†
University of Leeds, Leeds LS2 9JT, UK

Jean Hélder Marques Ribeiro‡
University of California, Los Angeles, CA 90095, USA

Chi-An Yeh§
North Carolina State University, Raleigh, NC 27695, USA

Kunihiko Taira¶
University of California, Los Angeles, CA 90095, USA

A significant hurdle in the adoption of resolvent analysis is the singular value decomposition (SVD) of the large linear operators involved. A matrix sketching algorithm is used to extract the primary forcing and response modes, with their associated gain. The formulation of an iterative algorithm is shown to be able to calculate the SVD of the resolvent operator accurately. The sources of error due to the selection of a test vector are discussed and it is shown that an accurate calculation of the forcing and response modes can be obtained by utilizing a test vector corresponding to a single point. The strength of this algorithm is shown by calculating the resolvent modes for a flow over a NACA 0012 airfoil at a Reynolds number of 23,000. This method is shown to converge for an arbitrary selection of test vector, obtaining results in agreement with past studies of this flow.

I. Introduction

Modal analysis has become a widespread tool in fluid mechanics [1, 2, 3, 4, 5, 6, 7]. Among these modal decomposition techniques, resolvent analysis reveals the input-output relationship with respect to a mean flow of interest [8, 9, 10]. Resolvent analysis is based on the concept of a particular solution under forcing, as opposed to global stability analysis which focuses on the homogeneous solution [11]. For this reason, resolvent analysis provides insights on how the flow responds to harmonic input to the system as well as the transient dynamics [12, 13]. As flows are exposed to perturbations and forcing at all times, resolvent analysis becomes a very attractive tool for characterizing, modeling, and controlling high-dimensional flows. Noteworthy here is that resolvent analysis can be performed about time-averaged turbulent base flows if the fluctuations about the base states are statistically stationary McKeon and Sharma [10], Farrell and Ioannou [14]. For these reasons, resolvent analysis stands out as essentially the only operator-based modal analysis technique that can handle practical engineering flows at high Reynolds numbers.

As a resolvent operator is spatially discretized, it can be represented by a matrix whose dimension is proportional to the number of spatial discretization points (grid size) and the number of state variables. The size of this matrix becomes very large for high-Reynolds number turbulent flows and especially for those without homogeneous directions (e.g., spatial periodicity). In such a case, computational challenges are encountered as the singular value decomposition of large-scale matrices demands significant computational resources and memory allocations.

Although the task of performing the resolvent analysis may seem daunting for large-scale flow problems, it should be noted that most fluid flow studies require only the dominant features of the flow to be revealed. That means that the amount of insights to be revealed is relatively small compared to the amount of data held by the large resolvent matrix.

*Graduate Research Assistant, Department of Mechanical and Aerospace Engineering, University of California, Los Angeles, CA 90095, USA
†Post-Doctoral Researcher, Department of Applied Mathematics, University of Leeds, Leeds LS2 9JT, UK
‡PhD Candidate, Department of Mechanical and Aerospace Engineering, University of California, Los Angeles, CA 90095, USA
§Assistant Professor, Department of Mechanical and Aerospace Engineering, North Carolina State University, Raleigh, NC 27695, USA
¶Professor, Department of Mechanical and Aerospace Engineering, University of California, Los Angeles, CA 90095, USA

This allows for the use of low-rank approximation of the large matrices to be considered to reduce the computational efforts necessitated by the singular value decomposition.

In particular we consider a technique referred to as *sketching* to extract the dominant characteristics of the original large-scale matrix. Sketching involves passing a test matrix comprised of a few linearly independent column vectors through the operator to be analyzed. The product of the original matrix and the test matrix holds important information about the action of the original matrix on the test matrix. In other words, the product should capture the dominant vectors in the range of the original matrix. The use of a random test matrix for determining appropriate rank reduction has resulted in the establishment of the randomized numerical linear algebra, which has become an active area of research in recent years.

In the present work, we place our focus on the choice of test matrix or test vector for the resolvent analysis and how it can be chosen based on the base flow. Furthermore, we demonstrate that in certain cases the singular value decomposition may be eliminated from the randomized resolvent algorithm, which significantly reduces the computational burden.

We first examine the randomized resolvent algorithm and its effect on single test vectors. Through this analysis we are able to derive error expressions for the forcing and response modes and the gain. We then perform resolvent analysis using this algorithm for flow over a NACA 0012 airfoil using test random vectors, and vectors corresponding to a single point in the flow. We discuss how the error is affected by the choice of test vector as well as how the behavior described by the error expression derived earlier manifests in modes obtained through this method.

II. Methodology

A. General Resolvent Analysis

For an unsteady fluid flow, we can decompose the state vector $\boldsymbol{q}$ into a time-invariant base flow $\bar{\boldsymbol{q}}$ and the time-variant fluctuations $\boldsymbol{q'}$ as

$$\boldsymbol{q} = \bar{\boldsymbol{q}} + \boldsymbol{q'}. \tag{1}$$

The time-variant and time-invariant state vectors are related by the following equation

$$\frac{\partial \boldsymbol{q'}}{\partial t} = \boldsymbol{L}_{\bar{\boldsymbol{q}}}\boldsymbol{q'} + \boldsymbol{f}, \tag{2}$$

where $\boldsymbol{L}_{\bar{\boldsymbol{q}}}$ is the linearized Navier–Stokes operator and $\boldsymbol{f}$ represents the collection of nonlinear terms, which can be interpreted as an internal forcing [10]. We can analyze the frequency response of the flow through analyzing the Fourier transform of equation (2)

$$-i\omega\hat{\boldsymbol{q}}_\omega = \boldsymbol{L}_{\bar{\boldsymbol{q}}}\hat{\boldsymbol{q}}_\omega + \hat{\boldsymbol{f}}_\omega. \tag{3}$$

The frequency ω can be chosen to be real for stable $\boldsymbol{L}_{\bar{\boldsymbol{q}}}$ or complex as $\omega = \omega_r + i\beta$ for unstable $\boldsymbol{L}_{\bar{\boldsymbol{q}}}$, where ω_r and β are both real and β discounts the modal growth rate of $\boldsymbol{L}_{\bar{\boldsymbol{q}}}$ [15, 16]. By rearranging (3) we can obtain an operator that maps a forcing input to a response of the state vector $\boldsymbol{q}$ in the form of

$$\hat{\boldsymbol{q}}_\omega = \boldsymbol{A}\hat{\boldsymbol{f}}_\omega, \tag{4}$$

where

$$\boldsymbol{A} = [-i\omega\boldsymbol{I} - \boldsymbol{L}_{\bar{\boldsymbol{q}}}]^{-1}, \tag{5}$$

is the resolvent operator. We can write $\boldsymbol{A}$ as its singular value decomposition (SVD)

$$\boldsymbol{A} = \boldsymbol{U}\boldsymbol{\Sigma}\boldsymbol{V}^*. \tag{6}$$

Written in this form, $\boldsymbol{V}$ represents the primary directions in which forcings are most effective, referred to as forcing modes, $\boldsymbol{U}$ represents the response s these forcings will induce, referred to as response modes, and $\boldsymbol{\Sigma}$ represents the associated gains mapping between the forcing modes and the associated responses.

B. Randomized Resolvent Analysis

The size of the resolvent operator is proportional to the number of grid points used to discretize the flow field. For higher-Reynolds number flows, the grid needs to be well-refined making the resolvent operator large in its size, and hence makes it difficult to perform an SVD.

Algorithm 1: Randomized Resolvent Analysis [17]

Require: Discrete resolvent operator $\boldsymbol{A} \in \mathbb{C}^{m\times m}$

Function `randomized_resolvent(`k`)`**:**

1 $\boldsymbol{\Omega} \leftarrow$ `randn(`m`,`k`)` // generate random forcing vectors $\boldsymbol{\Omega}$

2 $\boldsymbol{Y} \leftarrow \boldsymbol{A\Omega}$ // sketching: obtain response vectors $\boldsymbol{Y}$ by passing $\boldsymbol{\Omega}$ to $\boldsymbol{A}$

3 $(\boldsymbol{Q}, \sim) \leftarrow$ `qr(`$\boldsymbol{Y}$`,0)` // obtain orthonormal response bases $\boldsymbol{Q}$ from $\boldsymbol{Y}$

4 $\boldsymbol{B} \leftarrow \boldsymbol{Q}^*\boldsymbol{A}$ // obtain forcing bases $\boldsymbol{B}$ by passing $\boldsymbol{Q}$ to $\boldsymbol{A}^*$

5 $(\sim, \sim, \boldsymbol{V}) \leftarrow$ `svd(`$\boldsymbol{B}$`)` // obtain forcing modes via reduced SVD of $\boldsymbol{B}$

6 $\boldsymbol{U}^{\boldsymbol{\Sigma}} \leftarrow \boldsymbol{AV}$ // obtain gain-scaled response modes $\boldsymbol{U}^{\boldsymbol{\Sigma}}$ by passing $\boldsymbol{V}$ to $\boldsymbol{A}$

for $j \leftarrow 1$ *to* k **do**

7 $\boldsymbol{\Sigma}_{j,j} \leftarrow$ `norm(`$\boldsymbol{U}^{\boldsymbol{\Sigma}}_{1:m,j}, 2$`)` // recover gain

8 $\boldsymbol{U}_{1:m,j} \leftarrow \boldsymbol{U}^{\boldsymbol{\Sigma}}_{1:m,j}/\boldsymbol{\Sigma}_{j,j}$ // obtain unit-norm response modes $\boldsymbol{U}$

end

return $(\boldsymbol{U},\boldsymbol{\Sigma},\boldsymbol{V})$

The randomized resolvent analysis can be used to reduce the computational cost and memory requirement associated with performing the SVD while producing accurate resolvent modes and gains [17]. The reduction in computational costs is accomplished by performing the SVD on a low-rank approximation $\boldsymbol{B}$ of the full resolvent operator $\boldsymbol{A}$ instead of on $\boldsymbol{A}$ itself. The first step towards obtaining the low-rank approximation is called *sketching*. In this most crucial part of the randomized resolvent analysis, a sketch matrix $\boldsymbol{Y}$ is generated by passing a tall and skinny test matrix $\boldsymbol{\Omega} \in \mathbb{R}^{m\times k}$ ($m \gg k$) through the resolvent operator as

$$\boldsymbol{Y} = \boldsymbol{A\Omega}. \tag{7}$$

Oftentimes, this test matrix $\boldsymbol{\Omega}$ is chosen to be a random matrix, $\boldsymbol{\Omega} = \texttt{rand}(m, k)$. The focus of the present study is to take a detailed look at this sketching process with respect to the accuracies of the recovered resolvent modes and gains and complement the randomized algorithm with physical insights.

The sketched matrix $\boldsymbol{Y}$ should contain the dominant effect of the operator $\boldsymbol{A}$. We perform the QR decomposition of $\boldsymbol{Y}$ to obtain a low-rank basis aligned with the primary actions (directions) of the resolvent operator $\boldsymbol{A}$

$$\boldsymbol{Y} = \boldsymbol{QR}. \tag{8}$$

We then project the resolvent operator $\boldsymbol{A}$ onto this low-rank basis, to obtain a low-rank approximation of the resolvent

$$\boldsymbol{B} = \boldsymbol{Q}^*\boldsymbol{A} \in \mathbb{C}^{k\times m} \tag{9}$$

We can then perform the SVD of this projected matrix $\boldsymbol{B}$

$$\boldsymbol{B} = \widetilde{\boldsymbol{U}}\boldsymbol{\Sigma}\boldsymbol{V}^*. \tag{10}$$

While $\widetilde{\boldsymbol{U}}$ is the left singular vectors, we can obtain more accurate response modes of $\boldsymbol{A}$ by right multiplying the resolvent operator by the forcing modes $\boldsymbol{V}$ yielding

$$\boldsymbol{Av} = \sigma\boldsymbol{u}, \tag{11}$$

Since the left singular vectors are unitary ($|\boldsymbol{u}| = 1$), we obtain

$$\sigma = \|\boldsymbol{Av}\|, \tag{12}$$

$$\boldsymbol{u} = \sigma^{-1}\boldsymbol{Av}. \tag{13}$$

This process is outlined in algorithm 1 and discussed in detail by Ribeiro et al. [17].

First the test matrix $\boldsymbol{\Omega}$ is passed through the resolvent in line 2 to form the sketch matrix $\boldsymbol{Y}$, whose columns represent responses to the k forcing vectors $\boldsymbol{\Omega}$. In this step, the forcings excite response modes associated with the largest gains. However, these excited response modes appear in every column of the sketch matrix, or equivalently the response vectors $\boldsymbol{Y}$. To extract the response modes, the response vectors $\boldsymbol{Y}$ are orthonormalized via a QR decomposition in line 3 to provide a set of orthogonal bases $\boldsymbol{Q}$ for the response modes. The resolvent operator $\boldsymbol{A}$ is then projected onto

those bases $\boldsymbol{Q}$ in line 4 to produce a low-rank projected operator $\boldsymbol{B}$, which holds the principal characteristics of $\boldsymbol{A}$. The forcing modes $\boldsymbol{V}$ are then extracted in line 5 through the SVD of forcing bases $\boldsymbol{B}$. These forcing modes are left multiplied by $\boldsymbol{A}$ to yield $\sigma\boldsymbol{u}$ in line 6 (viz. equation 11) and subsequently separated into σ and $\boldsymbol{u}$ by using the unitary nature of the singular vectors in lines 7 and 8 (viz. equation 13). This randomized resolvent analysis algorithm has been demonstrated to perform well even with $k \ll m$ to determine the forcing modes, response modes, and gain while retaining its numerical accuracy.

C. Iterative Sketching Algorithm

Let us take a detailed look at sketching within the randomized resolvent analysis, algorithm 1. In line 1, we form a random test matrix $\boldsymbol{\Omega} \in \mathbb{R}^{m\times k}$, which can be considered as being comprised of k random forcing vectors in the length of the state variable m. We take this perspective to derive an iterative formulation, in which we utilize the forcing modes obtained by the algorithm as test matrix for the next iteration. In what follows, we seek an algorithm that finds the primary forcing and response modes along with the largest singular value through an iterative formulation.

Sketching plays the most important role in the algorithm of the randomized resolvent analysis. The test matrix $\boldsymbol{\Omega}$ initiates the sketching process with the attempt of exciting modes with the largest gains. If this attempt is successful, the rest of the algorithm shall produce the optimal gains and the associated forcing and response modes, yielding an accurate SVD. As a matter of fact, the test matrix $\boldsymbol{\Omega}$ is the tunable input we have control over in the randomized resolvent analysis. The choice of $\boldsymbol{\Omega}$ is crucial in producing accurate resolvent modes and gains, and we can rely on physical insights of the problem to improve the design of $\boldsymbol{\Omega}$.

A random matrix is intuitively the first choice for the test matrix $\boldsymbol{\Omega}$, if one has little knowledge about the physics of the operator [18]. Since a random $\boldsymbol{\Omega}$ can be interpreted as white forcing, it excites all response modes and allows those with highest gains to be amplified when being passed through the resolvent operator. However, better choices for $\boldsymbol{\Omega}$ can be made with the physical knowledge of the problem. Ribeiro et al. [17] considered a physics-informed test matrix based on the velocity gradient of the base flow and showed that the use of such test matrices can further enhance the accuracy of the randomized analysis with fewer number of vectors. Their demonstration showed great potential of leveraging flow physics in the design of test matrices.

We develop algorithm 2 by replacing the test matrix of algorithm 1 with a test vector, that is, a test matrix where $k = 1$. In this case, the sketch vector $\boldsymbol{y}$ contains the response bases for the forcing vector $\boldsymbol{\Omega}$. Since we only have a single vector to represent the response, there is no need for orthogonalization and we normalize the response $\boldsymbol{y}$ to obtain an approximation to the primary response mode. Similar to algorithm 1, we can determine the primary forcing basis by projecting the resolvent operator onto the response mode based on

$$\boldsymbol{A}^*\boldsymbol{u}_i = \sigma_i \boldsymbol{v}_i. \tag{14}$$

Due to the usage of a test vector, performing the SVD is not necessary and reduces to a simple normalization in algorithm 2. From here, we can once again utilize equation 11 to extract the response mode with greater accuracy. Since the response and forcing modes may not be accurate with a single evaluation, we then resort to an iterative procedure for lines 1 to 4. For the iterative process, the forcing mode from the previous iteration is used as the test vector for the following iteration, establishing algorithm 2.

Algorithm 2 considers a user-selected test vector as the test matrix $\boldsymbol{\Omega}$. If we define the inner product $\alpha_i \equiv \langle \boldsymbol{v}_i, \boldsymbol{\Omega}\rangle$, we can show that

$$\boldsymbol{y} = \sum_{i=1}^{m} \sigma_i \alpha_i \boldsymbol{u}_i^{\text{exact}} \tag{15}$$

where $\boldsymbol{u}_i^{\text{exact}}$ is the exact ith response mode. From this, we can determine an expression for $\boldsymbol{b}^*$

$$\boldsymbol{b}^* = \frac{1}{||\boldsymbol{y}||} \sum_{i=1}^{m} \sigma_i^2 \alpha_i \boldsymbol{v}_i^{\text{exact}}. \tag{16}$$

The forcing mode can be found by simply normalizing $\boldsymbol{v}_i$

$$\boldsymbol{v}_1 = \boldsymbol{b}^*/\|\boldsymbol{b}^*\|. \tag{17}$$

We recover the response mode and its gain by multiplying $\boldsymbol{v}$ by the resolvent operator to obtain

$$\sigma_1 \boldsymbol{u}_1 = \frac{1}{||\boldsymbol{b}||} \sum_{i=1}^{m} \sigma_i^3 \alpha_i \boldsymbol{u}_i^{\text{exact}} \tag{18}$$

Algorithm 2: Resolvent Analysis with a test vector $\boldsymbol{\Omega}$ (iterative)

Require: Discrete linear operator $\boldsymbol{L}_{\bar{\boldsymbol{q}}} \in \mathbb{C}^{m\times m}$, test vector $\boldsymbol{\Omega} \in \mathbb{C}^{m\times 1}$

Function `test_vector_resolvent(`ω`):`

for $i = 1$ *to* N **do**

1 $\quad \boldsymbol{y} \leftarrow \left[-i\omega\boldsymbol{I} - \boldsymbol{L}_{\bar{\boldsymbol{q}}}\right] \backslash \boldsymbol{\Omega}$ // solve linear system for $\boldsymbol{y}$

2 $\quad \boldsymbol{q} \leftarrow \boldsymbol{y}/\|\boldsymbol{y}\|_2$ // normalize $\boldsymbol{y}$

3 $\quad \boldsymbol{b} \leftarrow \boldsymbol{q}^*/\left[-i\omega\boldsymbol{I} - \boldsymbol{L}_{\bar{\boldsymbol{q}}}\right]$ // solve linear system for $\boldsymbol{b}$

4 $\quad \boldsymbol{\Omega} \leftarrow \boldsymbol{b}^*/\|\boldsymbol{q}\|_2$ // normalize $\boldsymbol{b}$ and transpose

end

5 $\boldsymbol{v} \leftarrow \boldsymbol{\Omega}$ // set $\boldsymbol{V}$ to $\boldsymbol{\Omega}$

6 $\boldsymbol{u}^{\boldsymbol{\Sigma}} \leftarrow \left[-i\omega\boldsymbol{I} - \boldsymbol{L}_{\bar{\boldsymbol{q}}}\right] \backslash \boldsymbol{v}$ // solve linear system to recover $\boldsymbol{u}^{\boldsymbol{\Sigma}}$

7 $\sigma \leftarrow \|\boldsymbol{u}^{\boldsymbol{\Sigma}}\|_2$ // recover gain

8 $\boldsymbol{u} \leftarrow \boldsymbol{u}^{\boldsymbol{\Sigma}}/\sigma$ // recover response mode

return $(\boldsymbol{u},\sigma,\boldsymbol{v})$

The main feature of this test vector based algorithm is that we make only a single attempt to initially excite the optimal responses. This prompts the question of how this test vector should be chosen. As previously discussed, Ribeiro et al. [17] suggested that the mean-flow physics should inform the choice. In this study, we will take this idea to its extreme by considering the case where the test vector $\boldsymbol{\Omega}$ is comprised of forcing at a single spatial point. We will later examine the effectiveness of this test vector with respect to the location of forcing. With the single-point test vector, we will use the iterative approach in algorithm 2 where the right singular vector obtained by the algorithm is then reused as the test vector for N iterations of this procedure.

We can apply equations 15-18 to the iterative form of the algorithm and substitute the values of $||\boldsymbol{y}||$ and $||\boldsymbol{b}||$ to obtain

$$\mathbf{v} = \frac{\sum_{i=1}^{m} \sigma_i^{2N} \alpha_i^* \boldsymbol{v}_i}{\sqrt{\sum_{i=1}^{m} \sigma_i^{4N} |\alpha_i|^2}}, \tag{19}$$

$$\sigma\boldsymbol{u} = \frac{\sum_{i=1}^{m} \sigma_i^{2N+1} \alpha_i^* \boldsymbol{u}_i}{\sqrt{\sum_{i=1}^{m} \sigma_i^{4N} |\alpha_i|^2}}, \tag{20}$$

$$\sigma^2 = \frac{\sum_{i=1}^{m} \sigma_i^{4N+2} |\alpha_i|^2}{\sum_{i=1}^{m} \sigma_i^{4N} |\alpha_i|^2}. \tag{21}$$

These expressions show the dependence of the output of the algorithm on all the singular values, and also on the initial test vector via α_i. Picking the test vector to perfectly align with the leading forcing mode would give $\alpha_i = \delta_{i1}$ and these expressions would then give the singular triplet $(\sigma_1, \boldsymbol{u}_1, \boldsymbol{v}_1)$ with no error. To examine the effect of a non-perfect choice we will make the assumption that the resolvent operator is low-rank. This will mean that $\sigma_1 \gg \sigma_2 \gg \ldots \gg \sigma_N$. This assumption allows us to Taylor expand the above expressions to give an estimate of the error in the obtained modes.

$$\|\boldsymbol{v} - \boldsymbol{v}_1\|^2 \approx \sum_{i=2}^{m} \frac{\sigma_i^{4N} |\alpha_i|^2}{\sigma_1^{4N} |\alpha_1|^2}, \tag{22}$$

$$\|\boldsymbol{u} - \boldsymbol{u}_1\|^2 \approx \sum_{i=2}^{m} \frac{\sigma_i^{4N+2} |\alpha_i|^2}{\sigma_1^{4N+2} |\alpha_1|^2}, \tag{23}$$

$$\sigma \approx \sigma_1 - \frac{\sum_{i=2}^{m} \sigma_i^{4N} |\alpha_i|^2}{2\sigma_1^{4N-1} |\alpha_1|^2}. \tag{24}$$

While it is impractical to perform even a rough approximation of the error prior to performing the SVD, these expressions still provide valuable insight on the sources of error. From this we can see that at leading order the relative error for the

singular values $|\sigma - \sigma_1|/\sigma_1$ is $O(\sigma_2^{4N}/\sigma_1^{4N})$, for the forcing $\|\boldsymbol{v} - \boldsymbol{v}_1\|$ is $O(\sigma_2^{2N}/\sigma_1^{2N})$ and for the response $\|\boldsymbol{u} - \boldsymbol{u}_1\|$ is $O(\sigma_2^{2N+1}/\sigma_1^{2N+1})$.

This algorithm will produce much more accurate results for systems where $\sigma_1 \gg \sigma_2, \sigma_3, \sigma_4, \ldots$. This agrees with the observations in [17]. For cases where σ_1/σ_2 is sufficiently large, this algorithm will produce accurate results regardless of the test vector used, including random test vectors. While the magnitude of the singular values are purely system dependent, the test vector can be selected to minimize error. An ideal test vector is aligned perfectly with with the first order forcing mode. Realistically this is very difficult since the structure of the forcing modes cannot generally be known in advance. Instead we rephrase the problem as attempting to find a vector which is nearly orthogonal to all other modes except for the first, and due to the assumption that the resolvent operator is low rank, we are primarily interested in ensuring orthogonality to specifically the second order mode. By localizing the forcing in a region where the second order mode is weak we can minimize this source of error. As a result, we can obtain a more accurate approximation for flows where the first two modes are spatially separated.

Forcing a single point of the flow means that α_1 will be smaller than what could be obtained by using a global forcing, however if the point is chosen using some physical insight as to where the first order forcing mode should appear then α_1 should be significantly larger than α_2. Through careful selection of the test vector, accurate results can be obtained using a single point test vector.

III. Results

A. Problem setup

We consider the application of the present formulation to uncover the response characteristics of turbulent separated flow over a NACA0012 airfoil [19]. For the resolvent analysis, we consider the flow response with respect to the time-averaged turbulent base flow, which is obtained by a high-fidelity large-eddy simulation. The computation is performed for the flow over an airfoil at an angle of attack of $\alpha = 9^\circ$, a chord-based Reynolds number of $Re = U_\infty c/\nu = 23,000$, and a free-stream Mach number of $M_\infty = 0.3$. The flow is taken to be spanwise-periodic with an extent of $0.2c$.

A finite-volume compressible flow solver CharLES [20, 21] is used to perform the large-eddy simulation of the turbulent flow over the wing. This solver is second and third-order accurate in space and time, respectively, with the Vreman's model [22] implemented for the subgrid-scale model. The spatial domain is chosen to be $x/c \in [-19, 26]$, $y/c \in [-20, 20]$ and $z/c \in [-0.1, 0.1]$ in the streamwise, transverse, and spanwise directions, respectively, with the leading edge positioned at the origin. This computational domain is discretized with a C grid. We specify the freestream velocity and temperature at the far field and prescribe a no-slip adiabatic boundary condition on the wing surface. A sponge layer is applied over the outlet to enable outgoing disturbances to exit the domain without reflecting back towards the near wake of the wing.

The base flow visualized in figure 1 is obtained by taking the time and spanwise average of the turbulent flow. As the whole computational domain is not required for the resolvent analysis, we extract the base flow over $x/c \in [-15, 16]$ and $y/c \in [-12, 12]$. The discretization of the resolvent operator over this sub-domain results in a resolvent operator of size 0.75 million by 0.75 million, which will be used in the subsequent analysis. The computational setup and the simulated base flow have been verified and validated extensively, as reported in our past studies [17, 19].

B. Resolvent analysis

We first examine results from the resolvent sketching algorithm for two choices of sparse test vectors, and compare the results obtained to results obtained using two different random test vectors. The first sparse test vector contains non-zero values only for the entries corresponding to the point of with the highest ratio α_1/α_2, and zeros otherwise. All non-zero elements in the vector are equal such that $||\alpha|| = 1$. The second sparse test vector is similar in construction, with non-zero elements corresponding to point in the freestream. The points effectively represent the best and worst case scenarios for the selection of test vector. The random test vectors used are both generated using a random normal distribution, however one is additionally weighted according to the velocity gradient as described in [17]

Results from resolvent analysis at $St = 1, \beta = 0$ and $St = 6, \beta = 20\pi$ are summarized in figures 2 and 3. Both of these are cases in which the algorithm can potentially struggle as σ_1/σ_2 is not very large, ≈ 6 and 20 respectively. For the former case, all response modes converge by ten iterations, with results showing excellent agreement. A poorly chosen test point results in the forcing mode converging more slowly, not converging by the tenth iteration. However selecting a test point at the location of the maximum velocity gradient results in the solution converging, and once again

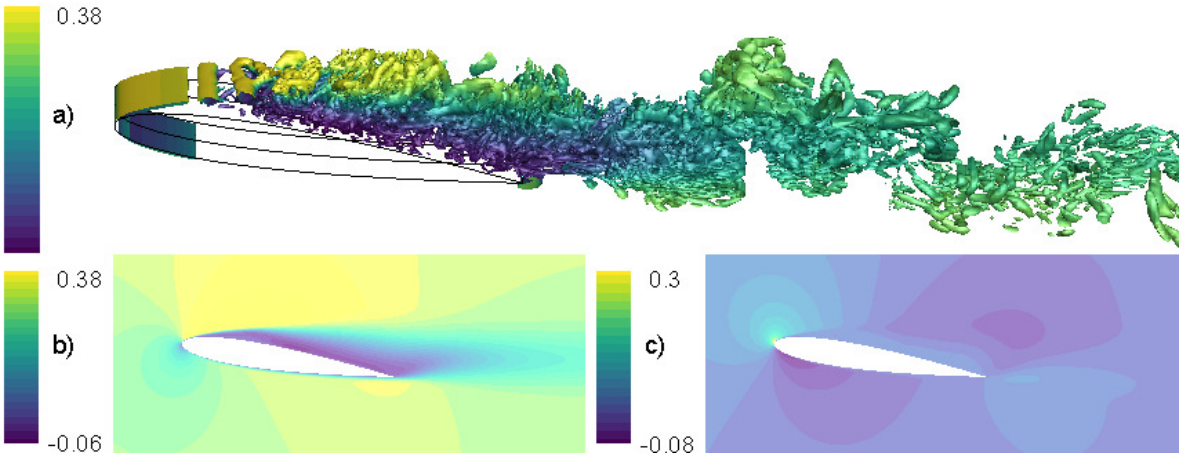

Fig. 1 Flow over a NACA 0012 airfoil at a Reynolds number of 23,000 and and a Mach number of 0.3 visualized by the Q-criterion isosurfaces (a). Time-averaged flows for the u (b) and v (c) components of velocity.

obtains excellent agreement with the exact solution. Of all the methods, a single test point near the leading edge of the airfoil performs best after a single iteration, while a single test point in the wake performs the worst, as it is unable to excite the first order forcing mode at all.

For the $St = 6, \beta = 20\pi$ case, the results follow a similar pattern. After the first iteration, the random test vector, gradient weighted random test vector, and the single point near the leading edge are already very difficult to distinguish, in agreement with the results of Ribeiro et al. [17] The single point forcing near the wake is unable to excite the forcing mode, however by the tenth iteration also results in an accurate solution. While the random test vector has been shown to work consistently, a single point test vector can obtain even better performance when chosen correctly as it can more precisely target purely the first order mode.

Convergence behavior of the iterative algorithm is shown in figures 4 and 5. The convergence rate for all methods follows the theoretical predictions, depending only on the ratio σ_1/σ_2. The convergence rate for some high error test vectors demonstrates odd behavior for the initial iterations, since the error is so large in these cases that the simplifying assumption used in the Taylor expansion of the error formula is no longer valid. For the $St = 6, \beta = 20\pi$ case, the wake test vector actually converges slower than the $St = 1, \beta = 0$ case despite a higher σ_1/σ_2. Early on the error for this case is dominated by the spatial discrepancy between the test vector and the forcing mode resulting in a value of $\alpha_1/\alpha_2 \approx 10^{-6}$. In order for the solution to converge the test vector in future iterations must overlap with the structure of the forcing mode, which is more difficult in the $\beta = 20\pi$ case as the size of the forcing mode is much smaller.

While the convergence rate is indeed similar for all methods, the choice of sketch vector can have a dramatic impact on the initial error, with a single sketch point placed at the leading edge of the airfoil has an error of order $< 10^{-5}$ while a randomized vector has an error of 10^2 for $St = 1, \sigma_1/\sigma_2 \approx 6$. For cases with ratios $\sigma_1/\sigma_2 \approx 1$, poorly chosen test vectors can struggle to converge, however proper selection of the test vector can result in convergence after only 1 or 2 iterations.

We additionally examine the error and convergence behavior of the algorithm for a selection of points on the surface of the NACA 0012 airfoil located at the leading and trailing edge, as well as the half chord on the pressure and suction side. The first iteration error depends on the ratio α_1/α_2. The spatial distribution of this ratio, as well as the test points examined on the surface are presented in figure 6. The first order forcing mode is primarily located near the leading edge of the airfoil, extending over the suction side, resulting in the test points in those regions outperforming the pressure side and trailing edge cases by several orders of magnitude, as presented in figure 7. While the initial error strongly depends on the selection of test point, all cases converge at the same rate due to the independence of the convergence rate from α_1/α_2. The convergence rate is instead problem specific, determined by the ratio in singular values σ_1/σ_2.

We also examine the structure of the forcing modes obtained after the first iteration in figure 8. The forcing mode calculated using the point placed at the leading edge is practically indistinguishable from the one obtained through the full SVD. The forcing mode calculated using the point at the trailing edge captures the primary features of the forcing mode, but also erroneous structures near the trailing edge. The additional structures are formed due the this point also exciting the second order mode, which is located primarily in the wake. The forcing modes calculated using this point

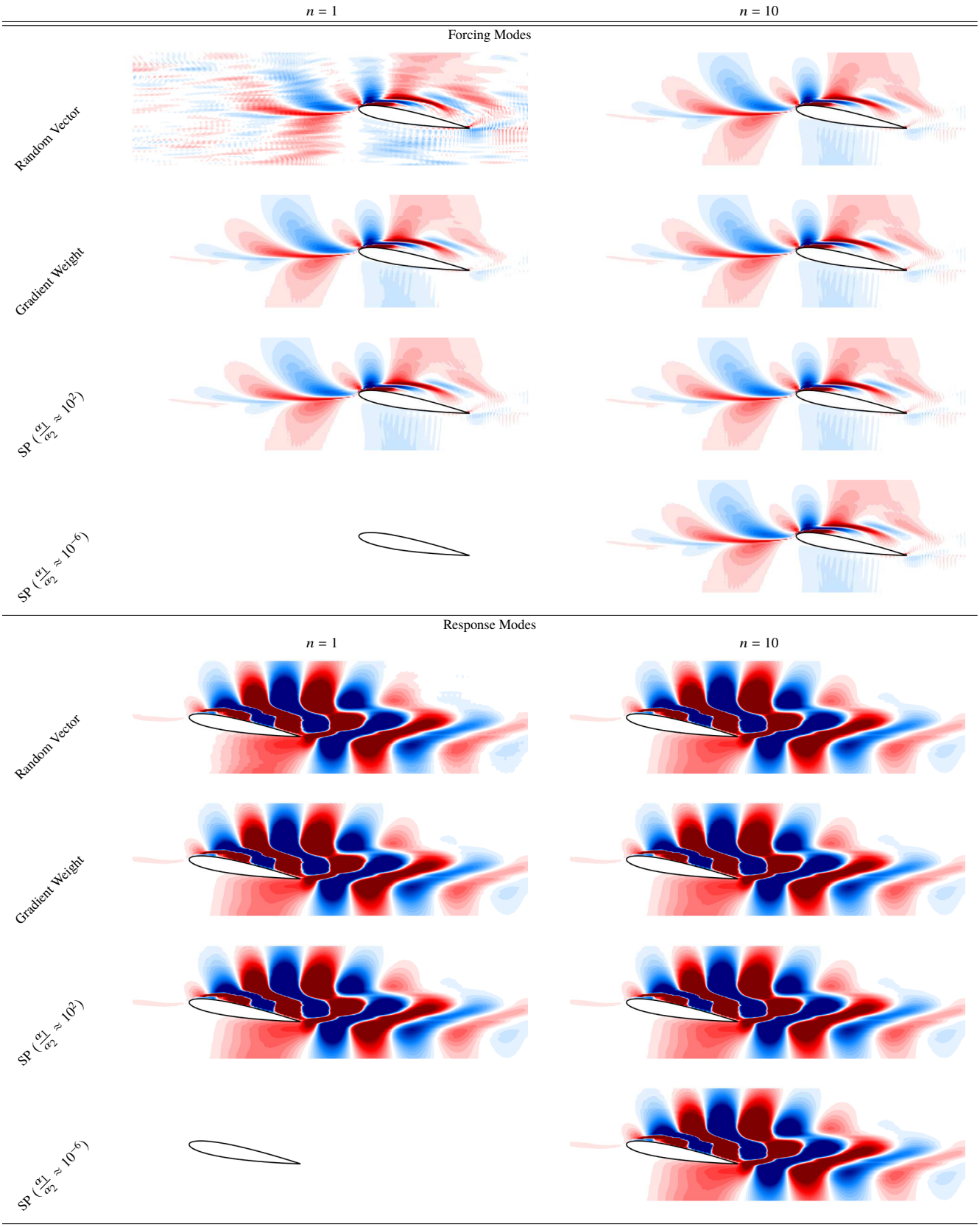

Fig. 2 Forcing and Response modes at $St = 1, \beta = 0$ for different types of test vectors after 1 and 10 iterations

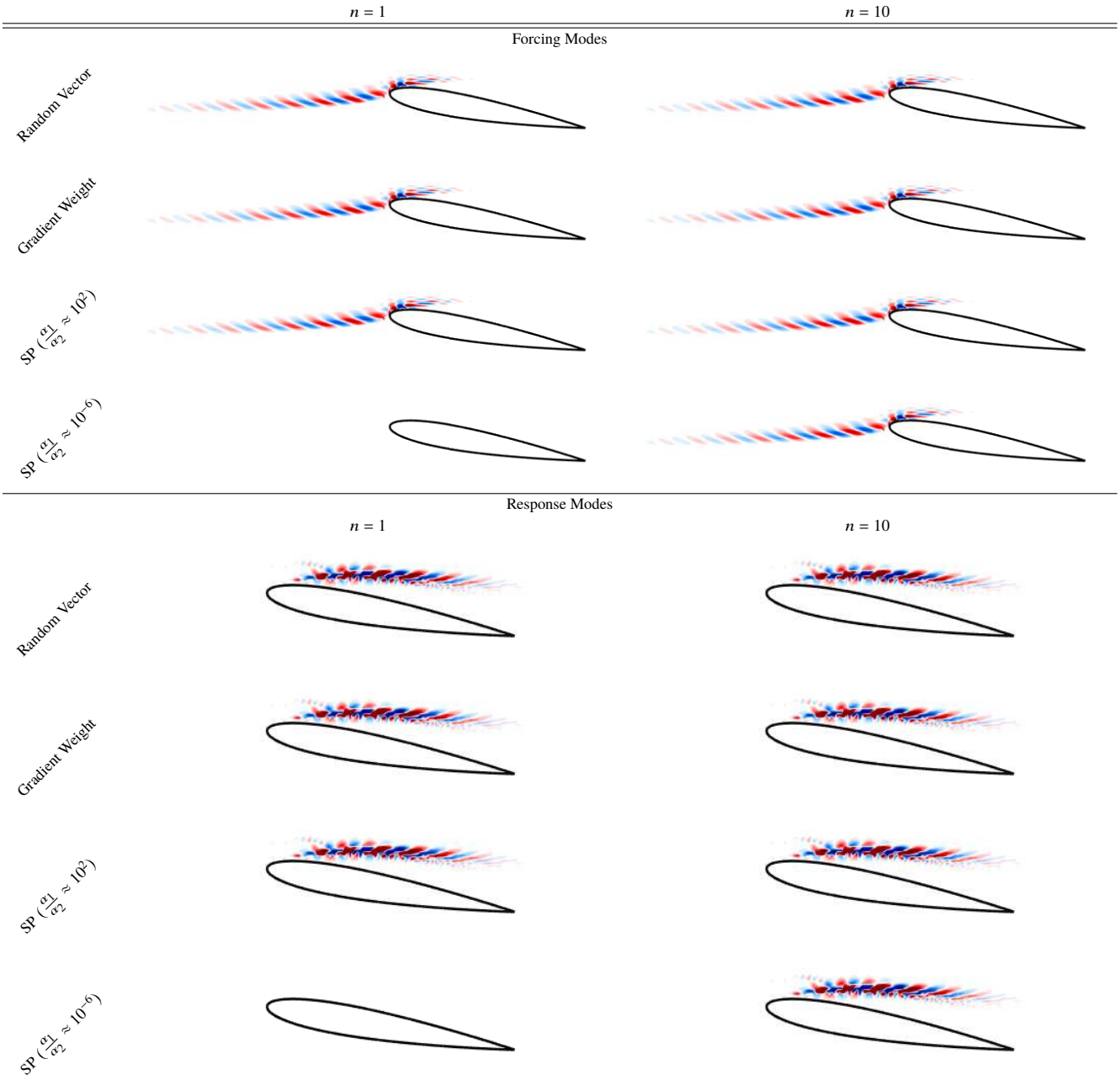

Fig. 3 Forcing and Response modes at $St = 6, \beta = 20\pi$ for different types of test vectors after 1 and 10 iterations

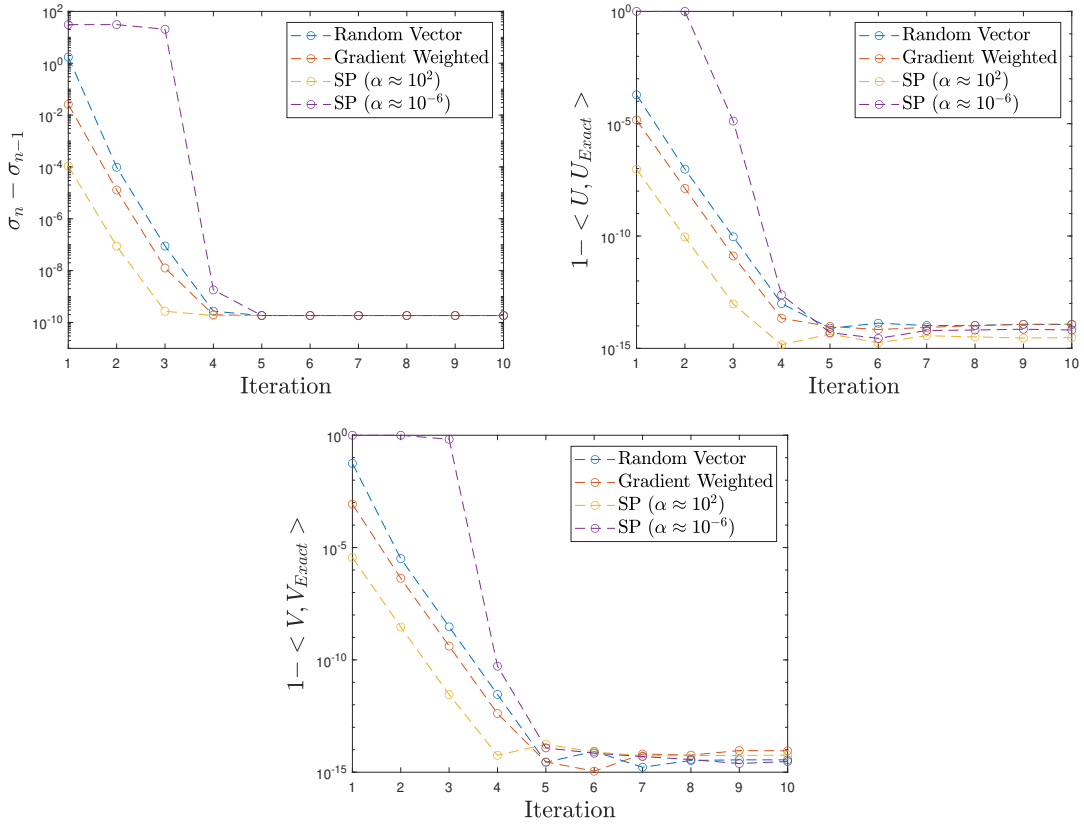

Fig. 4 Singular value error; Cosine similarity error of response modes; Cosine similarity error of forcing modes for $St = 1, \beta = 0$

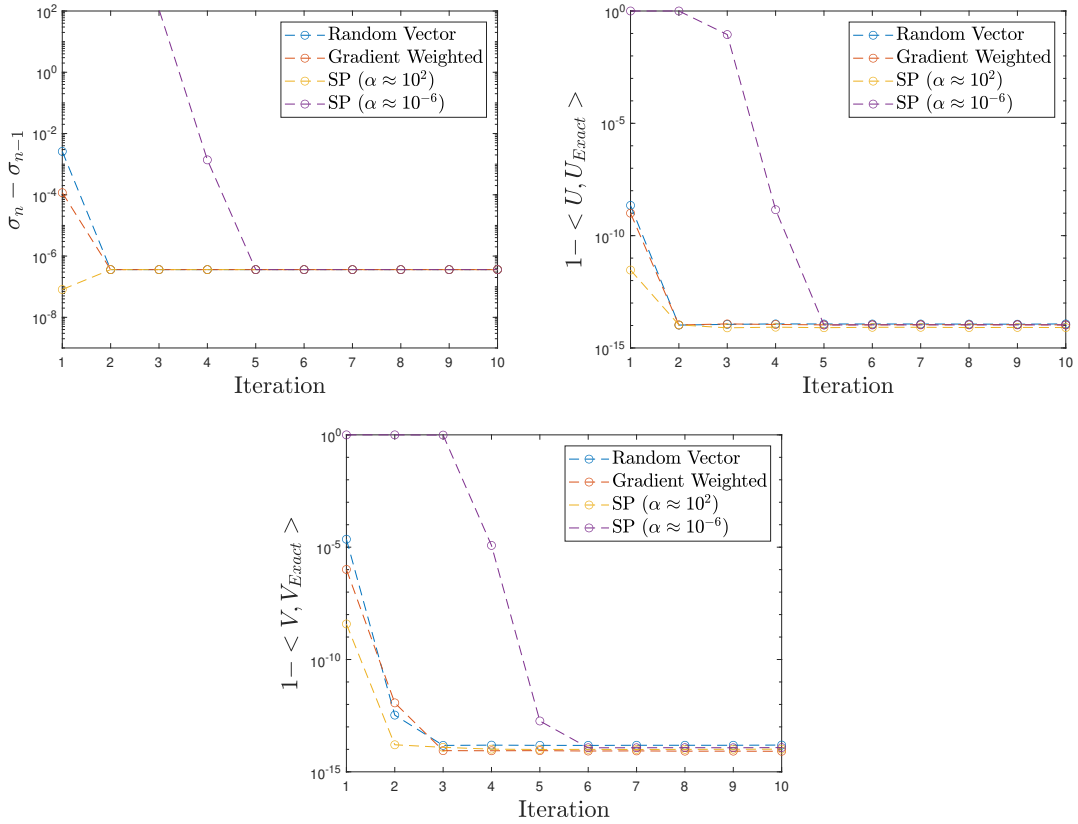

Fig. 5 Singular value error; Cosine similarity error of response modes; Cosine similarity error of forcing modes for $St = 6, \beta = 20\pi$

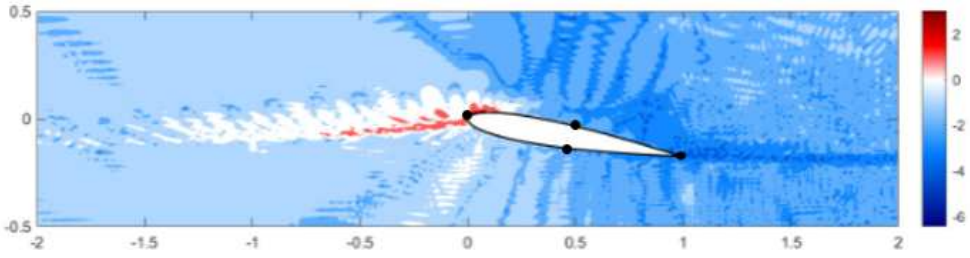

Fig. 6 Plot of α_1/α_2 depending on the single point forcing. Color bar is in log scale.

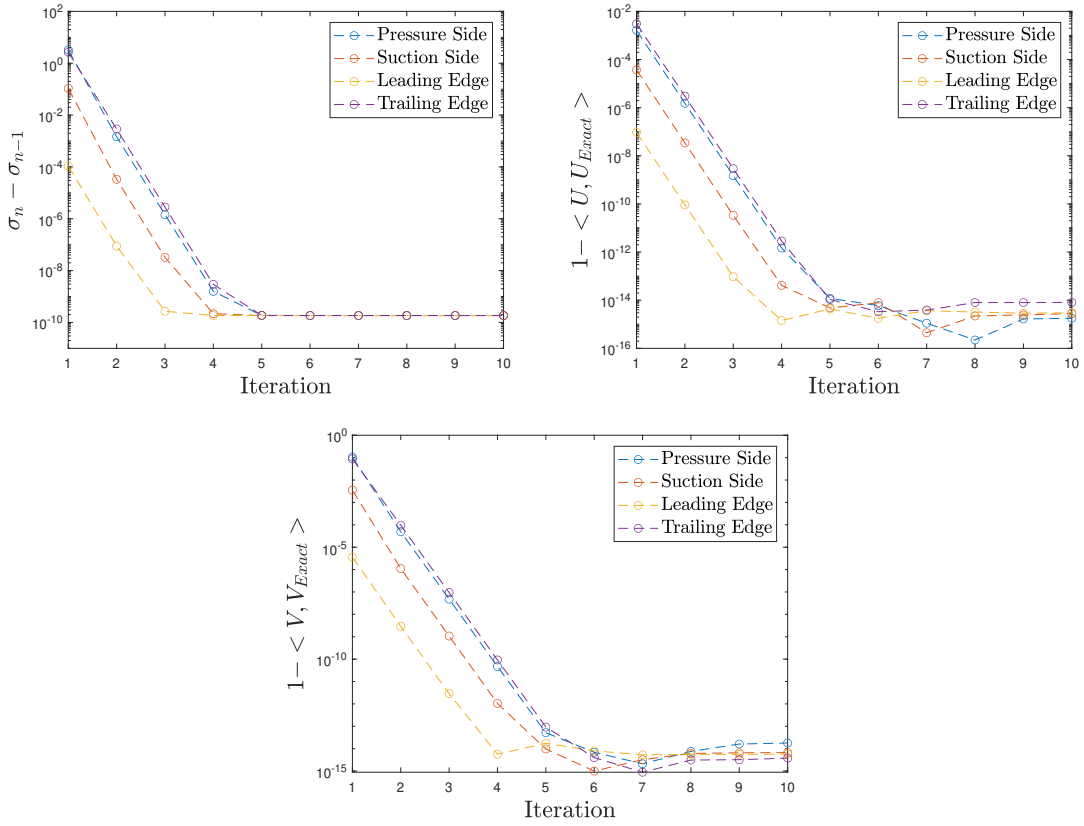

Fig. 7 Singular value error; Cosine similarity error of response modes; Cosine similarity error of forcing modes for a collection of test vectors on the airfoil surface

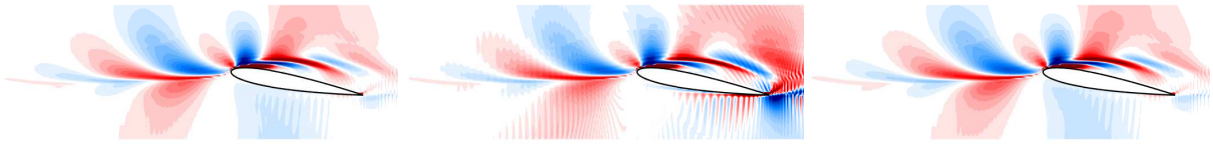

Fig. 8 Forcing Modes calculated using a point at the leading edge, a point at the trailing edge, and the full SVD respectively

are therefore a superposition of the first two modes. The vector containing the leading edge point is nearly orthogonal to the second order forcing mode while also aligning much more closely with the first mode, dramatically improving the accuracy of the result.

IV. Conclusion

While resolvent analysis has been shown to be a powerful tool in design of fluid control systems, the computational burden of performing the SVD on the resolvent operator can be a significant hurdle in its implementation. Sketching the resolvent operator can significantly reduce the computation time and memory requirements of the SVD. While a randomized test matrix is suitable for many cases, performance can be improved through careful selection of the a test vector when higher order modes are not necessary. Using a test vector makes it relatively simple to examine how exactly the sketching process affects the accuracy of the algorithm. The error analysis of the algorithm suggest that the test matrix can be sparse without a loss in performance. We show that when properly selected, a single point test vector can outperform a full test vector.

An important term in the error analysis is the inner product $\alpha_1 = \langle V_1 \Omega \rangle$. The improvement of the accuracy for test vectors more closely aligned with the forcing mode leads us to formulate this algorithm as an iterative process, where the test vector in the next step is the forcing mode calculated in the current step. Utilizing this iterative algorithm we can obtain results in excellent agreement with traditional SVD methods using arbitrary test vectors, with the number of iterations necessary for convergence significantly reduced by careful selection of the initial test vector.

Acknowledgements

This work was supported by the Army Research Office (grant: W911NF-21-1-0060, program officer: Matthew J. Munson) and the US Office of Naval Research (Program Manager: Dr. David Gonzalez, Grant number: N00014-19-1-2460). We thank Prof. Peter Schmid for enlightening discussions on resolvent analysis. Some of the computations presented here were supported by the Department of Defense High Performance Computing Modernization Program.

References

[1] Berkooz, G., Holmes, P., and Lumley, J. L., "The Proper Orthogonal Decomposition in the Analysis of Turbulent Flows," *Annual Review of Fluid Mechanics*, Vol. 25, No. 1, 1993, pp. 539–575.

[2] Holmes, P., Lumley, J. L., Berkooz, G., and Rowley, C. W., *Turbulence, coherent structures, dynamical systems and symmetry*, 2nd ed., Cambridge Univ. Press, 2012.

[3] Schmid, P. J., "Dynamic mode decomposition of numerical and experimental data," *J. Fluid Mech.*, Vol. 656, 2010, pp. 5–28.

[4] Kutz, J. N., *Data-driven modeling and scientific computation*, Oxford Univ. Press, 2013.

[5] Theofilis, V., "Global linear instability," *Annu. Rev. Fluid Mech.*, Vol. 43, 2011, pp. 319–352.

[6] Taira, K., Brunton, S. L., Dawson, S. T. M., Rowley, C. W., Colonius, T., McKeon, B. J., Schmidt, O. T., Gordeyev, S., Theofilis, V., and Ukeiley, L. S., "Modal analysis of fluid flows: An overview," *AIAA J.*, 2017, pp. 4013–4041.

[7] Taira, K., Hemati, M. S., Brunton, S. L., Sun, Y., Duraisamy, K., Bagheri, S., Dawson, S., and Yeh, C.-A., "Modal Analysis of Fluid Flows: Applications and Outlook," *AIAA J.*, 2019.

[8] Farrell, B. F., and Ioannou, P. J., "Stochastic forcing of the linearized Navier–Stokes equations," *Physics of Fluids A: Fluid Dynamics*, Vol. 5, No. 11, 1993, pp. 2600–2609.

[9] Trefethen, L. N., Trefethen, A. E., Reddy, S. C., and Driscoll, T. A., "Hydrodynamic stability without eigenvalues," *Science*, Vol. 261, No. 5121, 1993, pp. 578–584.

[10] McKeon, B. J., and Sharma, A. S., "A critical-layer framework for turbulent pipe flow," *J. Fluid Mech.*, Vol. 658, 2010, pp. 336–382.

[11] Schmid, P. J., "Nonmodal Stability Theory," *Annual Review of Fluid Mechanics*, Vol. 39, No. 1, 2007, pp. 129–162. https://doi.org/10.1146/annurev.fluid.38.050304.092139, URL https://doi.org/10.1146/annurev.fluid.38.050304.092139.

[12] Jovanovic, M. R., and Bamieh, B., "Componentwise energy amplification in channel flows," *J. Fluid Mech.*, Vol. 534, 2005, pp. 145–183.

[13] Trefethen, L. N., and Embree, M., *Spectra and pseudospectra*, Princeton Univ. Press, 2005.

[14] Farrell, B. F., and Ioannou, P. J., "Variance maintained by stochastic forcing of non-normal dynamical systems associated with linearly stable shear flows," *Physical Review Letters*, Vol. 72, 1994, pp. 1188–1191. URL https://link.aps.org/doi/10.1103/PhysRevLett.72.1188.

[15] Jovanović, M. R., "Modeling, analysis, and control of spatially distributed systems," Ph.D. thesis, University of California at Santa Barbara, Dept. of Mechanical Engineering, 2004.

[16] Yeh, C.-A., Benton, S. I., Taira, K., and Garmann, D. J., "Resolvent Analysis of an Airfoil Laminar Separation Bubble at $Re = 500,000$," *Physical Review Fluids*, Vol. 5, 2020, p. 083906. https://doi.org/10.1103/PhysRevFluids.5.083906.

[17] Ribeiro, J. H. M., Yeh, C.-A., and Taira, K., "Randomized resolvent analysis," *Phys. Rev. Fluids*, Vol. 5, 2020, p. 033902.

[18] Halko, N., Martinsson, P.-G., and Tropp, J. A., "Finding structure with randomness: Probabilistic algorithms for constructing approximate matrix decompositions," *SIAM review*, Vol. 53, No. 2, 2011, pp. 217–288.

[19] Yeh, C.-A., and Taira, K., "Resolvent-analysis-based design of airfoil separation control," *J. Fluid Mech.*, Vol. 867, 2019, pp. 572–610.

[20] Khalighi, Y., Nichols, J. W., Ham, F., Lele, S. K., and Moin, P., "Unstructured Large Eddy Simulation for Prediction of Noise Issued from Turbulent Jets in Various Configurations," 17th AIAA/CEAS Aeroacoustics Conference, 2011.

[21] Brès, G. A., Ham, F. E., Nichols, J. W., and Lele, S. K., "Unstructured Large-Eddy Simulations of Supersonic Jets," *AIAA J.*, Vol. 55, No. 4, 2017, pp. 1164–1184.

[22] Vreman, A. W., "An eddy-viscosity subgrid-scale model for turbulent shear flow: algebraic theory and applications," *Phys. Fluids*, Vol. 16, No. 10, 2004, pp. 3670–3681.